Class. Quantum Grav. **15** (1998) 481–500. Printed in the UK PII: S0264-9381(98)81279-3

Evaluation of a proposed test of the Weak Equivalence Principle using Earth-orbiting bodies in high-speed co-rotation

Y Jafry† and M Weinberger‡

† Space Science Department, ESTEC, Noordwijk, The Netherlands

‡ Automation and Informatics Department, ESTEC, Noordwijk, The Netherlands

Received 24 January 1997, in final form 3 September 1997

Abstract. The proposed space mission Galileo Galilei (GG) utilizes Earth-orbiting test masses in high-speed co-rotation to test the Weak Equivalence Principle (EP). This paper presents the results of a technical evaluation of the proposal, as it was presented in September 1996. Investigation of the dynamics and control aspects reveals that the experiment is limited by the imperfections inherent in the practical implementation of the required drag-free control and stabilizing servo forces. The net consequence is a degradation of the EP measurement sensitivity by many orders of magnitude compared with the proposers' expectations.

PACS numbers: 0480C, 0787, 0710Y

1. Introduction

The Galileo Galilei (GG) proposal [1–3] aims to test the Weak Equivalence Principle (EP) in space using Earth-orbiting test bodies co-rotating with an angular velocity of 5 Hz normal to the orbital plane. The rapid rotation is proposed in order to shift the frequency of the science signal away from the orbital frequency where sensor noise is typically more severe. It is claimed that the self-centring properties of elastically connected bodies spinning faster than the passive natural frequencies of the system (i.e. in 'supercritical rotation') can be beneficial to the experiment. As shown schematically in [1–3], the proposed system consists of six cylindrically symmetric bodies connected by a nested arrangement of springs and gimbals. The outer body is the spacecraft bus. Inside, suspended by weak springs, is the experiment chamber ('pico-gravity box' or PGB). The two test masses are suspended inside the PGB by weak springs attached to the ends of two rods, which, themselves, are connected to the PGB by weak gimbal springs affording two degrees of freedom of angular motion for each rod. The entire system spins at 5 Hz around the symmetry axis. Ideally, there is no relative rotational motion between the bodies. The putative EP signal is to be detected by measuring the relative translational displacements in two orthogonal directions between the two test masses using capacitive sensors. The experiment operates at room temperature. Drag-free control [4] using FEEP (field-effect electric propulsion) ion thrusters is proposed for attenuating the drag forces acting on the outer spacecraft body, though the early versions of the GG concept did not include drag-free control [5].

It is well known that dissipation co-rotating with the spinning bodies (i.e. 'rotating damping') leads to instability at supercritical speeds. In many situations (e.g. ground-based

0264-9381/98/030481+20$19.50

rotating machinery) this instability is passively suppressed by the action of 'non-rotating' damping forces arising from interaction between the spinning system and the non-spinning (inertial) environment. For the free-flying spinning satellite, there is effectively no such contact with the inertial frame. Active servo forces must therefore be applied between the bodies to provide the stabilization.

In the simplified analysis of the proposers, it is assumed that the required forces can be applied in an ideal manner. This fails to account for the disturbances introduced by scale-factor errors, misalignments and noise in the sensors and actuators. This paper addresses these issues, and demonstrates that the errors associated with the practical implementation of 'non-rotating damping' and drag-free control are a major limiting factor on the achievable performance. Under realistic assumptions, the Equivalence Principle measurement sensitivity is found to be $\eta \approx 10^{-14}$, where η is the Eötvös ratio defined as the fractional difference between the gravitational and inertial mass. In contrast, the GG proposers claim an expected sensitivity of $\eta \approx 10^{-17}$. The current limit from ground-based experiments is $\eta \approx 10^{-12}$ [6].

2. Dynamic modelling and control analysis

2.1. Notation

The spacecraft bus is represented by body A, the PGB by body B, the outer test mass by body C and the inner test mass by body D. These bodies have masses m_A, m_B, etc and inertias about their nominal spin axes I_A, I_B, etc. The inertial frame is denoted as N. Each body has a reference frame fixed in it. These are denoted as $[\vec{a}_1, \vec{a}_2, \vec{a}_3]$ for body A, $[\vec{b}_1, \vec{b}_2, \vec{b}_3]$ for body B, etc, and $[\vec{n}_1, \vec{n}_2, \vec{n}_3]$ for the inertial frame. The nominal spin axis is in the direction $\vec{n}_3$ which is nominally perpendicular to the orbital plane. The orbital frequency is much lower than the spin frequency and the elastic frequencies, and therefore the dynamical effects of orbital motion are very small and have been neglected to simplify the analysis.

Effective masses and inertias for pairwise coupled bodies are denoted with multiple subscripts. For example, for the coupled pair A and B, the effective mass and moment of inertia about the spin axis are

$$m_{AB} \triangleq \frac{m_A m_B}{m_A + m_B}, \qquad I_{AB} \triangleq \frac{I_A I_B}{I_A + I_B}. \tag{1}$$

All the passive forces between bodies are modelled as springs which provide displacement-dependent restoring forces, plus effective total viscous dissipation (from the springs and any other loss mechanism) which provides rate-dependent forces. Double subscripts are again employed. For example k_{AB} and c_{AB} represent the effective stiffness and viscous damping in the connections between A and B. The effective natural frequency and damping ratio for a pair of bodies are defined accordingly. For example,

$$\omega_{AB} \triangleq \sqrt{\frac{k_{AB}}{m_{AB}}}, \qquad \zeta_{AB} \triangleq \frac{c_{AB}}{2\omega_{AB} m_{AB}}, \qquad \zeta_{AB} \triangleq \frac{1}{2Q^V_{AB}} \tag{2}$$

characterize the translational couplings between A and B. As shown, the damping factors are conventionally defined in terms of effective viscous Q factors where the 'V' superscript emphasizes that all the losses are modelled as effective viscous losses. The determination of the suitable values for Q^V to be used in the equations of motion depends on expressing all the loss processes in the system in terms of equivalent viscosity. This is discussed in detail in the appendix.

Passive rotational stiffness and damping is represented in the same way as for translation, but with an additional θ subscript. For example, $k_{\theta_{\mathrm{AB}}}$ and $c_{\theta_{\mathrm{AB}}}$ represent the passive torsional stiffness and damping between bodies A and B.

Drag forces and torques acting on body A are naturally expressed in the inertial frame:

$$D_x\vec{n}_1 + D_y\vec{n}_2, \qquad D_\theta\vec{n}_3 \tag{3}$$

where D_x is the main drag term (i.e. opposite to the spacecraft velocity vector), D_y is the lift force due to the Magnus Effect and D_θ is the primary component of aerodynamic torque. Out-of-plane effects are ignored.

The drag-free control forces and torques acting on body A are naturally expressed in the spacecraft frame:

$$F_x^{\mathrm{dfc}}\vec{a}_1 + F_y^{\mathrm{dfc}}\vec{a}_2, \qquad F_\theta^{\mathrm{dfc}}\vec{a}_3. \tag{4}$$

The putative EP violation is modelled as a differential force acting between the test masses (bodies C and D). It is naturally expressed in the inertial frame as

$$F^{\mathrm{EP}}\vec{n}_2 \tag{5}$$

and is nominally oriented 90° from the main drag term.

The active servo forces acting between pairs of bodies are denoted with double superscripts to indicate the bodies, and a subscript to indicate direction. They are naturally expressed in the PGB body-fixed frame. For example, the servo force and torque vectors applied on body B by body A are given by

$$F_x^{\mathrm{AB}}\vec{b}_1 + F_y^{\mathrm{AB}}\vec{b}_2, \qquad F_\theta^{\mathrm{AB}}\vec{b}_3. \tag{6}$$

Equal and opposite forces and torque are applied on body A by body B.

The variables describing the dynamical motion are best written with respect to the PGB frame, because this is the frame in which the sensors are fixed. Thus, the position vectors from the spacecraft mass centre to the PGB mass centre; from the PGB mass centre to the outer test mass centre and from the PGB mass centre to the inner test mass centre are given by

$$x_{\mathrm{AB}}\vec{b}_1 + y_{\mathrm{AB}}\vec{b}_2, \qquad x_{\mathrm{BC}}\vec{b}_1 + y_{\mathrm{BC}}\vec{b}_2, \qquad x_{\mathrm{BD}}\vec{b}_1 + y_{\mathrm{BD}}\vec{b}_2 \tag{7}$$

respectively. Likewise, the position vector from the outer test mass to the inner test mass is given by

$$\Delta x\,\vec{b}_1 + \Delta y\,\vec{b}_2 \triangleq (x_{\mathrm{BD}} - x_{\mathrm{BC}})\vec{b}_1 + (y_{\mathrm{BD}} - y_{\mathrm{BC}})\vec{b}_2 \tag{8}$$

and these represent the two components of the differential measurement which contains the science signal (plus noise).

It is sometimes convenient to express the coordinates of the individual bodies and their relative positions with respect to the inertial frame. The superscript 'n' is used consistently for this purpose. A single subscript is used for an individual body, and a double subscript is used for the relative position of two bodies. For example, the position of body A with respect to the origin (arbitrary point, fixed in inertial space), and the position vector from body A to body B, are given by the inertial coordinates

$$^n x_{\mathrm{A}}\vec{n}_1 + {}^n y_{\mathrm{B}}\vec{n}_2, \qquad {}^n x_{\mathrm{AB}}\vec{n}_1 + {}^n y_{\mathrm{AB}}\vec{n}_2. \tag{9}$$

In the planar simplification, each body has only one degree of freedom in attitude. Denoting this as 'rotation', then the rotational angle of body A with respect to inertial space is denoted by θ_{A}. Similarly, the rotational angle of body B with respect to body A is denoted by θ_{AB}, etc.

The hat symbol is used to denote an estimate or measurement of a quantity, and the overbar symbol is used to denote the mean (average value) of a quantity. For example, $\hat{x}_{\mathrm{AB}}$ represents an estimate or measurement of x_{AB} (e.g. from a sensor), and $\bar{F}_x^{\mathrm{dfc}}$ represents the mean (or 'DC'†) value of F_x^{dfc}. Table 1 contains nominal numerical values for the various system parameters, derived from the GG literature.

Table 1. Nominal parameter values (see the appendix for a discussion on Q values). All torsional damping negligible ($c_{\theta_{\mathrm{AB}}} = c_{\theta_{\mathrm{BC}}} = c_{\theta_{\mathrm{BD}}} \approx 0$).

Mass (kg)	$m_{\mathrm{A}} = 120.6762$	$m_{\mathrm{B}} = 45.3803$	$m_{\mathrm{C}} = 10.0018$	$m_{\mathrm{D}} = 10.0001$
Inertias (kg m^2)	$I_{\mathrm{A}} = 28.9286$	$I_{\mathrm{B}} = 3.2543$	$I_{\mathrm{C}} = 0.0754$	$I_{\mathrm{D}} = 0.0165$
Stiffnesses (N m^{-1})	$k_{\mathrm{AB}} = 0.02$	$k_{\mathrm{BC}} = 0.02$	$k_{\mathrm{BD}} = 0.02$	$k_{\mathrm{CD}} = -0.005$
Effective viscous damping	$Q^{\mathrm{V}}_{\mathrm{AB}} = 5$	$Q^{\mathrm{V}}_{\mathrm{BC}} = Q^{\mathrm{V}}_{\mathrm{BD}} = 500$ (nominal) $Q^{\mathrm{V}}_{\mathrm{BC}} = Q^{\mathrm{V}}_{\mathrm{BD}} = 2.5 \times 10^4$ (high) $Q^{\mathrm{V}}_{\mathrm{BC}} = Q^{\mathrm{V}}_{\mathrm{BD}} = 2.5 \times 10^5$(extreme)		$Q^{\mathrm{V}}_{\mathrm{CD}} \approx \infty$
Torsional stiffnesses (N m rad^{-1})	$k_{\theta_{\mathrm{AB}}} = k_{\theta_{\mathrm{BC}}} = k_{\theta_{\mathrm{BD}}} = 6.25 \times 10^{-6}$			

2.2. Two-body planar model

The minimal dynamic model that captures some of the essential features of the GG system consists of two bodies, each with three degrees of freedom (two planar translational, one rotational) as depicted in figure 1. The mounting points of all springs on all bodies will generally not pass through their respective centres of mass, and it is important to incorporate these offsets when generating the equations of motion. In order to understand the consequences on the dynamics (at least for the planar simplification) it is only necessary to include one such offset without much loss of generality. The location on body A where the springs are attached is denoted as a_{s}, which is offset from the centre of mass of A by the vector

$$\varepsilon_x^{\mathrm{AB}}\vec{a}_1 + \varepsilon_y^{\mathrm{AB}}\vec{a}_2 \tag{10}$$

as depicted in figure 1. The other end of the spring is assumed to be attached to the centre of mass of B. The passive forces acting on body B through its centre of mass are

$$-\left(k_{\mathrm{AB}}\left(x_{\mathrm{AB}} - \varepsilon_x^{\mathrm{AB}}\right) + c_{\mathrm{AB}}\dot{x}_{\mathrm{AB}}\right)\vec{a}_1 - \left(k_{\mathrm{AB}}\left(y_{\mathrm{AB}} - \varepsilon_y^{\mathrm{AB}}\right) + c_{\mathrm{AB}}\dot{y}_{\mathrm{AB}}\right)\vec{a}_2 \tag{11}$$

and the passive forces acting on body A through point a_{s} are

$$\left(k_{\mathrm{AB}}\left(x_{\mathrm{AB}} - \varepsilon_x^{\mathrm{AB}}\right) + c_{\mathrm{AB}}\dot{x}_{\mathrm{AB}}\right)\vec{a}_1 + \left(k_{\mathrm{AB}}\left(y_{\mathrm{AB}} - \varepsilon_y^{\mathrm{AB}}\right) + c_{\mathrm{AB}}\dot{y}_{\mathrm{AB}}\right)\vec{a}_2. \tag{12}$$

It is assumed that the drag-free control forces are applied by thrusters mounted on A, acting through the centre of mass of A, and that the active 'non-rotating damping' servo forces are applied through the centres of mass of A and B.

2.2.1. Equilibrium offsets between spacecraft and PGB. The equilibrium ('trim') condition for a nominal spin rate Ω can be determined from the nonlinear equations of motion for

† The expression 'DC' used here and elsewhere in the text should be understood to imply 'very low frequency' compared with the signal frequency, e.g. the drag forces are effectively DC in inertial space, neglecting the orbital motion.

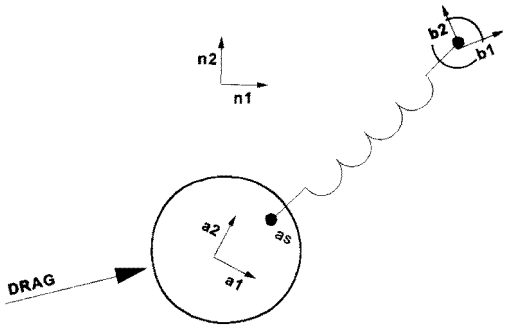

Figure 1. Two-body planar model: spacecraft plus PGB.

the system (not reproduced here). The resulting offset vector describing the steady-state separation between the centres of mass is given by

$$\bar{x}_{\mathrm{AB}}\vec{a}_1 + \bar{y}_{\mathrm{AB}}\vec{a}_2 \tag{13}$$

where $\bar{x}_{\mathrm{AB}}$, $\bar{y}_{\mathrm{AB}}$ are the solution of the linear equation

$$\begin{aligned}
&\begin{pmatrix} -\Omega^2 + \dfrac{K_{\mathrm{P}}^{\mathrm{dfc}}}{m_{\mathrm{A}}} + \dfrac{k_{\mathrm{AB}}}{m_{\mathrm{AB}}} & -\Omega\left[\dfrac{K_{\mathrm{D}}^{\mathrm{dfc}}}{m_{\mathrm{A}}} + \dfrac{C_{\mathrm{AB}}}{m_{\mathrm{AB}}}\right] \\ \Omega\left[\dfrac{K_{\mathrm{D}}^{\mathrm{dfc}}}{m_{\mathrm{A}}} + \dfrac{C_{\mathrm{AB}}}{m_{\mathrm{AB}}}\right] & -\Omega^2 + \dfrac{K_{\mathrm{P}}^{\mathrm{dfc}}}{m_{\mathrm{A}}} + \dfrac{k_{\mathrm{AB}}}{m_{\mathrm{AB}}} \end{pmatrix} \begin{pmatrix} \bar{x}_{\mathrm{AB}} \\ \bar{y}_{\mathrm{AB}} \end{pmatrix} \\
&\quad = \begin{pmatrix} \dfrac{k_{\mathrm{AB}}}{m_{\mathrm{AB}}} & 0 \\ 0 & \dfrac{k_{\mathrm{AB}}}{m_{\mathrm{AB}}} \end{pmatrix} \begin{pmatrix} \varepsilon_x^{\mathrm{AB}} \\ \varepsilon_y^{\mathrm{AB}} \end{pmatrix} \\
&\quad + \begin{pmatrix} -\dfrac{K_{\mathrm{P}}^{\mathrm{dfc}}}{m_{\mathrm{A}}} & \Omega\left[\dfrac{K_{\mathrm{D}}^{\mathrm{dfc}}}{m_{\mathrm{A}}} + \dfrac{C_{\mathrm{AB}}}{m_{\mathrm{AB}}}\right] \\ -\Omega\left[\dfrac{K_{\mathrm{D}}^{\mathrm{dfc}}}{m_{\mathrm{A}}} + \dfrac{C_{\mathrm{AB}}}{m_{\mathrm{AB}}}\right] & -\dfrac{K_{\mathrm{P}}^{\mathrm{dfc}}}{m_{\mathrm{A}}} \end{pmatrix} \begin{pmatrix} \bar{n}_x^{\mathrm{AB}} \\ \bar{n}_y^{\mathrm{AB}} \end{pmatrix}
\end{aligned} \tag{14}$$

where C_{AB}, $K_{\mathrm{P}}^{\mathrm{dfc}}$, $K_{\mathrm{D}}^{\mathrm{dfc}}$ are the control gains for inter-body stabilization and drag-free control (described later in sections 2.2.4 and 2.3.2), and $\bar{n}_x^{\mathrm{AB}}$, $\bar{n}_y^{\mathrm{AB}}$ are the sensor biases. The steady-state distance between the centres of mass, and the angle between the nominal body axes and the axes defined by the steady-state vector, are then given by

$$\bar{\delta}r_{\mathrm{AB}} \triangleq \sqrt{\bar{x}_{\mathrm{AB}}^2 + \bar{y}_{\mathrm{AB}}^2}, \qquad \alpha_{\mathrm{offset}} = \tan^{-1}\left(\frac{\bar{y}_{\mathrm{AB}}}{\bar{x}_{\mathrm{AB}}}\right). \tag{15}$$

These relations only reduce to the well known results

$$\bar{\delta}r_{\mathrm{AB}} = -\frac{\varepsilon\omega_{\mathrm{AB}}^2}{\Omega^2 - \omega_{\mathrm{AB}}^2}, \qquad \alpha_{\mathrm{offset}} = 0 \tag{16}$$

when all the control forces are disabled (ε denotes the magnitude of the vector in equation (10)). In general, the bias control forces will not be zero because of sensor and actuator imperfections, resulting in a degradation of the supercritical centring. For example, with typical mounting-location offsets of $|\varepsilon_x^{\mathrm{AB}}|$, $|\varepsilon_y^{\mathrm{AB}}| \approx 10^{-4}$ m, sensor biases of 1 μm, and

with the control laws and gains described in later sections, the equilibrium offsets between the spacecraft mass centre and PGB mass centre are $\bar{\delta}r_{\mathrm{AB}} \approx 2 \times 10^{-6}$ m and $\alpha_{\mathrm{offset}} \approx 45^{\circ}$ in the case where both the drag-free control and the 'non-rotating damping' laws are active, with the nominal spin rate of 5 Hz ($\Omega \approx 31$ rad s^{-1}). These are dominated by the drag-free control bias forces. If only the 'non-rotating' damping is active (i.e. the drag-free control is switched off), the offsets become $\bar{\delta}r_{\mathrm{AB}} \approx 4 \times 10^{-7}$ m and $\alpha_{\mathrm{offset}} \approx 45^{\circ}$. As one referee of this paper pointed out, these effects may be slightly attenuated by using bandpass control. Nevertheless, the offsets are very large compared with the uncontrolled case where only the elastic term appears, yielding $\bar{\delta}r_{\mathrm{AB}} \approx 6 \times 10^{-11}$ m and $\alpha_{\mathrm{offset}} = 0$, as assumed by the proposers.

2.2.2. Equilibrium positions of the test masses. A similarly precise treatment for the test masses would involve lengthy expressions because of all the forces and couplings involved. A reasonable approximation can be obtained by treating the bodies in a pairwise manner, and adapting the results stated above by analogy. First consider the case with zero biases on the control forces. The equilibrium distance between the PGB and each test mass is then of the order of 2.5×10^{-10} m, and the distance between the test masses is of the order of 10^{-10} m. When the control force biases are included, the equilibrium distances between the PGB and each test mass are of the order of 3.5×10^{-9} m for the nominal Q assumption ($Q^{\mathrm{V}}_{\mathrm{BC}} = Q^{\mathrm{V}}_{\mathrm{BD}} = 500$), and 2.5×10^{-10} m for the extremely high-Q assumption ($Q^{\mathrm{V}}_{\mathrm{BC}} = Q^{\mathrm{V}}_{\mathrm{BD}} = 2.5 \times 10^{5}$, see the appendix). In all cases, the steady-state separations between the bodies are much larger than suggested by the proposers. In particular, the separation between the test masses is approximately six times larger, which will increase the centripetal forces, and amplify the adverse effects of three-dimensional dynamical couplings on the experiment. In order to achieve the levels of centring quoted in the proposal (1.67×10^{-11} m), the spin rate would have to be increased to 12 Hz, which would aggravate other disturbances, and may not even be feasible (5 Hz is already an unprecedented spin rate for a spacecraft).

2.2.3. Linearized equations of motion. In order to analyse the stability of the system at the equilibrium condition, it is necessary to linearize the equations of motion about the equilibrium. This is facilitated if the body axes are redefined by rotating them through the angle α_{offset}. Then, the steady-state offset is simply $\bar{\delta}r_{\mathrm{AB}}$ along the redefined $\vec{a}_1$ direction, and the linearized equations of motion are:

$$\begin{aligned} {}^{n}\ddot{x}_{\mathrm{A}} = {} & \big(\big(-F_x^{\mathrm{AB}} + F_x^{\mathrm{dfc}} + 2m_{\mathrm{AB}}\dot{x}_{\mathrm{AB}}\omega_{\mathrm{AB}}\zeta_{\mathrm{AB}} + \bar{\delta}r_{\mathrm{AB}}m_{\mathrm{AB}}\Omega^2 + m_{\mathrm{AB}}x_{\mathrm{AB}}\omega_{\mathrm{AB}}^2\big)\cos\Omega t \\ & + D_x + \big(F_y^{\mathrm{AB}} - F_y^{\mathrm{dfc}} - 2m_{\mathrm{AB}}\dot{y}_{\mathrm{AB}}\omega_{\mathrm{AB}}\zeta_{\mathrm{AB}} \\ & - m_{\mathrm{AB}}y_{\mathrm{AB}}\omega_{\mathrm{AB}}^2 - \bar{\delta}r_{\mathrm{AB}}m_{\mathrm{B}}\theta_{\mathrm{A}}\Omega^2\big)\sin\Omega t\big)/m_{\mathrm{A}} \end{aligned} \tag{17}$$

$$\begin{aligned} {}^{n}\ddot{y}_{\mathrm{A}} = {} & \big(D_y - \big(F_x^{\mathrm{AB}} - F_x^{\mathrm{dfc}} - 2m_{\mathrm{AB}}\dot{x}_{\mathrm{AB}}\omega_{\mathrm{AB}}\zeta_{\mathrm{AB}} - \bar{\delta}r_{\mathrm{AB}}m_{\mathrm{AB}}\Omega^2 - m_{\mathrm{AB}}x_{\mathrm{AB}}\omega_{\mathrm{AB}}^2\big)\sin\Omega t \\ & - \big(F_y^{\mathrm{AB}} - F_y^{\mathrm{dfc}} - 2m_{\mathrm{AB}}\dot{y}_{\mathrm{AB}}\omega_{\mathrm{AB}}\zeta_{\mathrm{AB}} \\ & - m_{\mathrm{AB}}y_{\mathrm{AB}}\omega_{\mathrm{AB}}^2 - \bar{\delta}r_{\mathrm{AB}}m_{\mathrm{B}}\theta_{\mathrm{A}}\Omega^2\big)\cos\Omega t\big)/m_{\mathrm{A}} \end{aligned} \tag{18}$$

$$\begin{aligned} \ddot{x}_{\mathrm{AB}} = {} & 2\dot{y}_{\mathrm{AB}}\Omega + F_x^{\mathrm{AB}}/m_{\mathrm{AB}} + 2\bar{\delta}r_{\mathrm{AB}}\dot{\theta}_{\mathrm{A}}\Omega - 2\dot{x}_{\mathrm{AB}}\omega_{\mathrm{AB}}\zeta_{\mathrm{AB}} \\ & - x_{\mathrm{AB}}\big(\omega_{\mathrm{AB}}^2 - \Omega^2\big) - \big(F_x^{\mathrm{dfc}} + D_x\cos\Omega t + D_y\sin\Omega t\big)/m_{\mathrm{A}} \end{aligned} \tag{19}$$

$$\ddot{y}_{\mathrm{AB}} = F_y^{\mathrm{AB}}/m_{\mathrm{AB}} + \bar{\delta}r_{\mathrm{AB}}\big(F_\theta^{\mathrm{AB}} - F_\theta^{\mathrm{dfc}} - D_\theta - c_{\theta_{\mathrm{AB}}}\dot{\theta}_{\mathrm{AB}} - k_{\theta_{\mathrm{AB}}}\theta_{\mathrm{AB}}\big)/I_{\mathrm{A}}$$
$$-y_{\mathrm{AB}}\big(\omega_{\mathrm{AB}}^2 - \Omega^2\big)\big(1 + m_{\mathrm{AB}}\bar{\delta}r_{\mathrm{AB}}^2/I_{\mathrm{A}}\big) - 2\dot{x}_{\mathrm{AB}}\Omega$$
$$-\big(F_y^{\mathrm{dfc}} + D_y\cos\Omega t - D_x\sin\Omega t\big)/m_{\mathrm{A}}$$
$$-2\dot{y}_{\mathrm{AB}}\zeta_{\mathrm{AB}}\big(\omega_{\mathrm{AB}} + m_{\mathrm{AB}}\bar{\delta}r_{\mathrm{AB}}^2(\omega_{\mathrm{AB}}^2 - \Omega^2)/(I_{\mathrm{A}}\omega_{\mathrm{AB}})\big) \tag{20}$$

$$\ddot{\theta}_{\mathrm{A}} = 2\bar{\delta}r_{\mathrm{AB}}m_{\mathrm{AB}}\dot{y}_{\mathrm{AB}}\zeta_{\mathrm{AB}}\big(\omega_{\mathrm{AB}}^2 - \Omega^2\big)/(I_{\mathrm{A}}\omega_{\mathrm{AB}}) - \bar{\delta}r_{\mathrm{AB}}m_{\mathrm{AB}}\big(\big(F_y^{\mathrm{AB}}/m_{\mathrm{AB}}\big) - \big(F_y^{\mathrm{dfc}}/m_{\mathrm{A}}\big)\big)/I_{\mathrm{A}}$$
$$-\big(F_\theta^{\mathrm{AB}} - F_\theta^{\mathrm{dfc}} - D_\theta - c_{\theta_{\mathrm{AB}}}\dot{\theta}_{\mathrm{AB}} - k_{\theta_{\mathrm{AB}}}\theta_{\mathrm{AB}} - \bar{\delta}r_{\mathrm{AB}}m_{\mathrm{AB}}y_{\mathrm{AB}}\big(\omega_{\mathrm{AB}}^2 - \Omega^2\big)\big)/I_{\mathrm{A}} \tag{21}$$

$$\ddot{\theta}_{\mathrm{AB}} = \big(F_\theta^{\mathrm{AB}} - c_{\theta_{\mathrm{AB}}}\dot{\theta}_{\mathrm{AB}} - k_{\theta_{\mathrm{AB}}}\theta_{\mathrm{AB}}\big)/I_{\mathrm{AB}} - \big(F_\theta^{\mathrm{dfc}} + D_\theta + \bar{\delta}r_{\mathrm{AB}}m_{\mathrm{AB}}y_{\mathrm{AB}}\big(\omega_{\mathrm{AB}}^2 - \Omega^2\big)\big)/I_{\mathrm{A}}$$
$$-2\bar{\delta}r_{\mathrm{AB}}m_{\mathrm{AB}}\dot{y}_{\mathrm{AB}}\zeta_{\mathrm{AB}}\big(\omega_{\mathrm{AB}}^2 - \Omega^2\big)/(I_{\mathrm{A}}\omega_{\mathrm{AB}}) \tag{22}$$

where it is understood that the control forces are redefined to have zero bias, and all variables are redefined as small perturbations relative to values of zero at trim, except for x_{AB} which is measured relative to the non-zero quantity $\bar{x}_{\mathrm{AB}} = \bar{\delta}r_{\mathrm{AB}}$ at trim.

The first two equations describe the inertial accelerations of body A. Although they are influenced by body B, they do not exert an influence on the remaining equations, and can be ignored for now. The next two equations describe the relative translational accelerations between the bodies (in body-fixed coordinates), and the final two equations describe the rotational dynamics.

The translational and rotational equations are coupled by virtue of the offset $\bar{\delta}r_{\mathrm{AB}}$. The quantity $\big(\Omega^2 - \omega_{\mathrm{AB}}^2\big)$ plays a pivotal role since some coefficients in the differential equations undergo a change of sign at supercritical speeds (i.e. when $\Omega > \omega_{\mathrm{AB}}$), indicating that stability can be affected. The simplest way to examine the stability of the system (at least for small motions about trim) is to evaluate the eigenvalues (poles). For the nominal system parameters and for $Q_{\mathrm{AB}}^{\mathrm{V}} = 5$, the offset distance is $\bar{\delta}r_{\mathrm{AB}} = 6 \times 10^{-11}$ m at 5 Hz, and the system poles are

$$\left.\begin{array}{l} -0.279\,9203 - 31.694\,46\mathrm{i} \\ -0.279\,9203 + 31.694\,46\mathrm{i} \\ +0.275\,0003 - 31.137\,39\mathrm{i} \\ +0.275\,0003 + 31.137\,39\mathrm{i} \end{array}\right\} \text{translational 'whirling' modes (rad s}^{-1}\text{)}$$

$$\left.\begin{array}{l} -1.110\,15 \times 10^{-9}\mathrm{i} \\ +1.110\,15 \times 10^{-9}\mathrm{i} \\ +1.368\,676 \times 10^{-10} \\ -1.368\,676 \times 10^{-10} \end{array}\right\} \text{rotational modes (rad s}^{-1}\text{).}$$

For larger values of $Q_{\mathrm{AB}}^{\mathrm{V}}$ (see the appendix) the growth (decay) of unstable (stable) modes will be slower. It is clear that two of the translational poles are unstable (often called 'unstable forward whirling modes'). This is to be expected at supercritical speeds if there is any effective damping between the co-rotating bodies [7]. It is of interest to note that the simplified model of the damping leads to frictional forces which are parallel, but not collinear, thus total angular momentum is not conserved. This explains why there are not at least two rotational poles exactly at the origin.

As well as the unstable whirling modes, one of the rotational poles is unstable (though very slow) due to coupling to translation. Furthermore, the stable poles are also very slow, implying that the bodies are essentially unconstrained in rotation. Hence, a small bias disturbance force of, say, 1 μN acting over a distance of 1 μm will produce a 10^{-4} rad relative rotation between the spacecraft and the PGB in about 2.5×10^4 s. This would be

unacceptable in terms of the consequent sensor and actuator alignment errors. Likewise, each test mass will drift in rotation relative to the PGB, but the growth rate is even faster: similar relative rotations will occur in about 3×10^3 s. The effect of initial rate errors is yet faster again. Even if the initial uncaging procedure could achieve rates as low as 10^{-7} rad s^{-1}, these will lead to intolerable rotations in 10^3 s. The springs may provide some passive rotational damping, but this will not be a sufficient restraint against large transient excursions. It is therefore concluded that each body must have active rotation control. Also, the translational dynamics of the PGB and the test masses along the spin axis are similarly very lightly damped and will require active control. With all these control systems, the GG system will be technically complex, in contrast to the proposers' claims that a key feature of the experiment is its simplicity.

Assuming for the present that the rotations are perfectly controlled, the rotational variables vanish from the equations of motion, leaving

$$\ddot{x}_{\mathrm{AB}} = 2\dot{y}_{\mathrm{AB}}\Omega - 2\dot{x}_{\mathrm{AB}}\omega_{\mathrm{AB}}\zeta_{\mathrm{AB}} - x_{\mathrm{AB}}\left(\omega_{\mathrm{AB}}^2 - \Omega^2\right) + F_x^{\mathrm{AB}}/m_{\mathrm{AB}} - \left(F_x^{\mathrm{dfc}} + D_x\cos\Omega t + D_y\sin\Omega t\right)/m_{\mathrm{A}} \tag{23}$$

$$\ddot{y}_{\mathrm{AB}} = -2\dot{x}_{\mathrm{AB}}\Omega - 2\dot{y}_{\mathrm{AB}}\zeta_{\mathrm{AB}}\omega_{\mathrm{AB}} - y_{\mathrm{AB}}\left(\omega_{\mathrm{AB}}^2 - \Omega^2\right) + F_y^{\mathrm{AB}}/m_{\mathrm{AB}} - \left(F_y^{\mathrm{dfc}} + D_y\cos\Omega t - D_x\sin\Omega t\right)/m_{\mathrm{A}} \tag{24}$$

where the $\bar{\delta}r_{\mathrm{AB}}^2$ terms have been neglected.

2.2.4. 'Non-rotating damping'. It is well known that the supercritical instabilities in the system of equations (23), (24) can be stabilized by the application of viscous damping relative to the inertial frame (i.e. 'non-rotating' damping). To implement such a control law, the forces applied between the bodies would be, in the inertial frame,

$$\vec{F}_{\mathrm{ideal}} = -C_{\mathrm{AB}}\left({}^n\dot{x}_{\mathrm{AB}}\vec{n}_1 + {}^n\dot{y}_{\mathrm{AB}}\vec{n}_2\right) \tag{25}$$

where C_{AB} is the desired viscous damping constant. This is the control strategy suggested in the GG proposal [1, 2], and is the basis of the present analysis. Alternative schemes, proposed more recently by various parties, are discussed briefly in section 2.2.7.

2.2.5. Practical implementation of control. For the free-flying system, the damping forces must be implemented using a feedback control law driven by measurements of the relative motion. Furthermore, there are no measurements of the relative motion in inertial space: all measurements are performed in the rotating frame since the (capacitive) sensors are fixed in the spacecraft. Therefore, the required inertial rates $\left({}^n\dot{x}_{\mathrm{AB}}, {}^n\dot{y}_{\mathrm{AB}}\right)$ in the ideal control law (equation (25)) must be re-constructed from body-fixed measurements. Similarly, the servo forces must be applied in the rotating frame, since the (electrostatic) servos are fixed in the spacecraft. By simple transformation of reference frames, the practical control law becomes

$$\begin{aligned}\vec{F}_{\mathrm{design}} &= F_x^{\mathrm{AB}}\vec{a}_1 + F_y^{\mathrm{AB}}\vec{a}_2 \\ &= -C_{\mathrm{AB}}((\dot{x}_{\mathrm{AB}} - \Omega y_{\mathrm{AB}})\vec{a}_1 + (\dot{y}_{\mathrm{AB}} + \Omega x_{\mathrm{AB}})\vec{a}_2).\end{aligned} \tag{26}$$

Substituting these into equations (23), (24), and determining the stability criterion yields

$$\frac{C_{\mathrm{AB}}}{c_{\mathrm{AB}}} > \frac{\Omega}{\omega_{\mathrm{AB}}} - 1 \approx \frac{\Omega}{\omega_{\mathrm{AB}}} \qquad \text{(for supercritical rotation).} \tag{27}$$

This is the same result as in the GG proposal [2], (using γ_{nr} for C_{AB}, and β_r for c_{AB}). Allowing for some margin above the stability limit, a suitable gain is

$$C_{\mathrm{AB}} = g_{\mathrm{AB}}c_{\mathrm{AB}}\frac{\Omega}{\omega_{\mathrm{AB}}} = g_{\mathrm{AB}}\frac{\sqrt{k_{\mathrm{AB}}m_{\mathrm{AB}}}}{Q_{\mathrm{AB}}^{\mathrm{V}}}\frac{\Omega}{\omega_{\mathrm{AB}}} \tag{28}$$

with the pre-factor $g_{AB} \approx 1.2$ (found to be reasonable from trial and error). Substitution of this into the control law (equation (26)) gives

$$F_x^{AB} = -g_{AB}c_{AB}\frac{\Omega}{\omega_{AB}}(\dot{x}_{AB} - \Omega y_{AB}), \qquad F_y^{AB} = -g_{AB}c_{AB}\frac{\Omega}{\omega_{AB}}(\dot{y}_{AB} + \Omega x_{AB}). \tag{29}$$

The control law imposes spring-like (position-dependent) forces due to gyroscopic coupling, as well as damping (rate-dependent) forces. Although these spring-like forces are applied across the phase-space (i.e. F_x^{AB} has a spring-like coupling to y_{AB}, and vice versa), they are real forces continuously applied to the bodies, and coupling to the same displacements (x_{AB}, y_{AB}) as the passive springs. Since noise contributions will generally be larger than the deterministic terms in equations (29), there will not be a near cancellation of the rate and gyroscopic components, as would occur in an ideal noise-free environment. It is therefore meaningful to use the following ratio:

$$F_{AB}^{ratio} \triangleq \frac{|\text{active spring force}|}{|\text{passive spring force}|} = \frac{g_{AB}}{Q_{AB}^V}\left(\frac{\Omega}{\omega_{AB}}\right)^2 \tag{30}$$

as an indication of the relative magnitude of the active and passive forces. For nominal parameter values ($g_{AB} = 1.2$, $\Omega \approx 31$ rad s^{-1}, $\omega_{AB} = 0.025$ rad s^{-1}, $Q_{AB}^V = 5$) the active forces are found to dominate the passive forces by $\approx 4 \times 10^5$ (see the appendix and section 2.3.6 for a discussion of the results for higher values of Q_{AB}^V). As will be discussed later, the control laws necessary to stabilize the motion of each test mass relative to the PGB can be designed using pairwise approximations analogous to the spacecraft–PGB pair just presented. The ratio of active to passive spring forces acting on the test masses can be similarly evaluated, and turns out to be $\approx 10^3$, for nominal parameter values. When noise is considered (see the next section), then even the static forces due to sensor biases exceed the passive spring forces by a factor of ≈ 20 for $Q_{BC}^V = Q_{BD}^V = 500$, and the dynamic active forces dominate by a factor of ≈ 500.

The entire GG system is thus dominated by servo forces, and the performance of the experiment will be determined by the accuracy to which the applied servo forces can be balanced across the test masses, and by the degree to which sensor noise propagates into the differential mode.

2.2.6. Sensor and actuator imperfections. To assess the errors due to non-ideal control, the measurements of x_{AB}, y_{AB}, $\dot{x}_{AB}$, $\dot{y}_{AB}$ must be modelled to include imperfections due to noise, scale-factor errors, misalignments, etc. Similarly, the actuator forces will not be perfectly applied, so the actual control law which takes effect will be

$$\begin{pmatrix} F_x^{AB} \\ F_y^{AB} \end{pmatrix} = -C_{AB}\begin{pmatrix} 1+\delta_{AB}^{F_x} & 0 \\ 0 & 1+\delta_{AB}^{F_y} \end{pmatrix}\begin{pmatrix} \cos\epsilon_{AB}^F & \sin\epsilon_{AB}^F \\ -\sin\epsilon_{AB}^F & \cos\epsilon_{AB}^F \end{pmatrix}\begin{pmatrix} \hat{\dot{x}}_{AB} - \Omega\hat{y}_{AB} \\ \hat{\dot{y}}_{AB} + \Omega\hat{x}_{AB} \end{pmatrix} \tag{31}$$

where $\delta_{AB}^{F_x}$, $\delta_{AB}^{F_y}$ are actuator scale-factor errors, ϵ_{AB}^F is the angular misalignment between the actuators and the sensors and the estimates of position ($\hat{x}_{AB}$, $\hat{y}_{AB}$) come directly from the sensors

$$\hat{x}_{AB} = \left(1+\delta_{AB}^{S_x}\right)\left(x_{AB} + n_x^{AB}\right), \qquad \hat{y}_{AB} = \left(1+\delta_{AB}^{S_y}\right)\left(y_{AB} + n_y^{AB}\right) \tag{32}$$

where n_x^{AB}, n_y^{AB} are additive noise, and $\delta_{AB}^{S_x}$, $\delta_{AB}^{S_y}$ are sensor scale-factor errors. Each noise component will generally comprise a DC bias plus a stochastic term. The DC biases will depend on geometrical as well as electrical factors. Ideally, the sensors should measure displacements relative to the equilibrium positions. However, as shown earlier, these equilibrium positions (described by $\bar{\delta}r_{AB}$, α_{offset}) will not be known because they will depend

on all the unknown elastic offsets in the system as well as on the bias forces. In fact, it is not at all clear how the sensors could even be calibrated relative to the true equilibrium offsets.

The rate estimates ($\hat{\dot{x}}_{AB}, \hat{\dot{y}}_{AB}$) must be approximated from the position measurements (since there are no rate sensors). The most straightforward method is to use a lead–lag network which yields

$$\hat{\dot{x}}_{AB} = \frac{S + 1/\tau_1}{\tau_2 S + 1}\hat{x}_{AB}, \qquad \hat{\dot{y}}_{AB} = \frac{S + 1/\tau_1}{\tau_2 S + 1}\hat{y}_{AB} \tag{33}$$

where 'S' is the Laplace variable, and τ_1, τ_2 are the time constants of the filter. These must be chosen to provide a derivative action at the signal frequency. While the lower break frequency ($1/\tau_1$) can be selected over a wide range below the signal frequency, stability dictates that the upper break frequency ($1/\tau_2$) should be large. Suitable values are found to be $\tau_1 \approx 10^4$ s and $\tau_2 \approx 5 \times 10^{-4}$ s. Servo force noise has been omitted because it is found to be negligible in comparison with sensor noise and drag.

2.2.7. Other control schemes. Subsequent to the analysis presented here, the GG proposers have suggested several alternative control schemes to circumvent the difficulties of the non-cancellation of large terms, inherent to their original suggestion, as described in section 2.2.5.

Motivated by the notion that in the ideal case the control effort required should only be that which exactly balances the very small destabilizing forces, they suggest to apply to each unstable differential whirling mode the following law, in place of equation (25):

$$F_{\text{ideal}} = C_{AB}\omega_{AB}r_w \tag{34}$$

where r_w is the magnitude of that mode as viewed from the inertial frame. If this ideal law were realizable, then indeed the active control forces would just balance the very small passive destabilizing forces, as also shown in equation (35) of [8]. However, this is an impractical idealization because each individual inertially referenced mode displacement r_w is virtually unobservable within the time constraints imposed by the stability requirements. For example, it is found that a lag of only 7% of the inertial whirl period can destabilize the system. This is not enough time to measure r_w with sufficient accuracy.

In an effort to approach the ideal law of equation (34), the proposers suggest to use an Earth elevation sensor (EES) to produce a smoothed spin-rate measurement which also serves as a master clock by which successive body-fixed displacement measurements are scheduled. Measurements separated by one spin period are then used after filtering to approximate the inertial rates which can be fed directly into equation (25). With this approach, the direct construction of individual gyroscopic and rate terms in equation (26) is circumvented. This technique has also been advocated by others [9]. However, in the realistic noisy environment with sensor and actuator scale-factor errors and misalignments, both approaches will suffer from comparable imperfections which cannot be avoided, though the new approach shifts some of the noise problems onto the spin-rate measurement (i.e. onto the EES for the spacecraft spin rate, and onto whatever sensors are used to measure the relative rotations between the inner bodies).

A related technique, suggested by one of the referees of this paper, would be to modify the control law in equation (26) by band-limiting the control around the unstable frequencies. While this reduces the sensor noise propagation to some extent, it does not eliminate it. The required control forces still completely dominate the passive damping forces, in contrast to the idealized law of equation (34).

2.3. Four-body planar model

In order to investigate how drag and sensor noise will couple into the differential displacements between the test masses, thus corrupting the EP measurement, it is necessary to consider a four-body model as depicted in figure 2 (where the equivalent 2D spring stiffnesses can be determined from consideration of the actual 3D rod–spring–gimbal geometry).

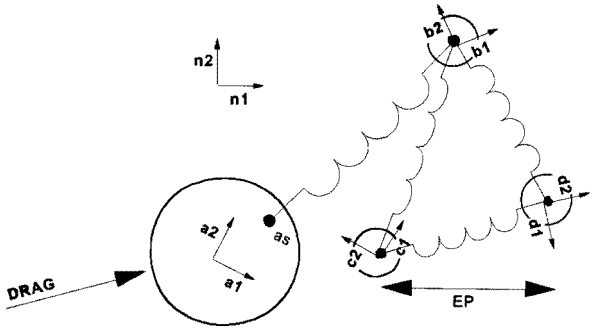

Figure 2. Four-body planar model: PGB, spacecraft, plus two test masses ('inner' and 'outer').

2.3.1. Linearized equations of motion. Proceeding as for the two-body model, the full nonlinear equations were derived, then linearized around the trim condition. These equations are long and tedious, and are not reproduced here. It is found that, again, the translation and rotational dynamics are coupled via the equilibrium offsets, and that both the translational and rotational subsystems contain instabilities at supercritical speeds. It is therefore essential to control the rotational modes of all bodies. Assuming this is achieved perfectly, the remaining translational dynamical equations are as follows:

$$\begin{aligned} {}^{n}\ddot{x}_{\mathrm{A}} = {} & \big(\big(-F_x^{\mathrm{AB}} + F_x^{\mathrm{dfc}} + c_{\mathrm{AB}}\dot{x}_{\mathrm{AB}} + k_{\mathrm{AB}}x_{\mathrm{AB}}\big)\cos\Omega t + D_x \\ & + \big(F_y^{\mathrm{AB}} - F_y^{\mathrm{dfc}} - c_{\mathrm{AB}}\dot{y}_{\mathrm{AB}} - k_{\mathrm{AB}}y_{\mathrm{AB}}\big)\sin\Omega t\big)/m_{\mathrm{A}} \end{aligned} \tag{35}$$

$$\begin{aligned} {}^{n}\ddot{y}_{\mathrm{A}} = {} & \big(D_y - \big(F_y^{\mathrm{AB}} - F_y^{\mathrm{dfc}} - c_{\mathrm{AB}}\dot{y}_{\mathrm{AB}} - k_{\mathrm{AB}}y_{\mathrm{AB}}\big)\cos\Omega t \\ & - \big(F_x^{\mathrm{AB}} - F_x^{\mathrm{dfc}} - c_{\mathrm{AB}}\dot{x}_{\mathrm{AB}} - k_{\mathrm{AB}}x_{\mathrm{AB}}\big)\sin\Omega t\big)/m_{\mathrm{A}} \end{aligned} \tag{36}$$

$$\begin{aligned} \ddot{x}_{\mathrm{AB}} = {} & 2\dot{y}_{\mathrm{AB}}\Omega + F_x^{\mathrm{AB}}/m_{\mathrm{AB}} - 2\dot{x}_{\mathrm{AB}}\omega_{\mathrm{AB}}\zeta_{\mathrm{AB}} - x_{\mathrm{AB}}\big(\omega_{\mathrm{AB}}^2 - \Omega^2\big) \\ & - \big(F_x^{\mathrm{dfc}} + D_x\cos\Omega t + D_y\sin\Omega t\big)/m_{\mathrm{A}} \\ & - \big(F_x^{\mathrm{BC}} + F_x^{\mathrm{BD}} - c_{\mathrm{BC}}\dot{x}_{\mathrm{BC}} - c_{\mathrm{BD}}\dot{x}_{\mathrm{BD}} - k_{\mathrm{BC}}x_{\mathrm{BC}} - k_{\mathrm{BD}}x_{\mathrm{BD}}\big)/m_{\mathrm{B}} \end{aligned} \tag{37}$$

$$\begin{aligned} \ddot{y}_{\mathrm{AB}} = {} & F_y^{\mathrm{AB}}/m_{\mathrm{AB}} - 2\dot{x}_{\mathrm{AB}}\Omega - 2\dot{y}_{\mathrm{AB}}\omega_{\mathrm{AB}}\zeta_{\mathrm{AB}} - y_{\mathrm{AB}}\big(\omega_{\mathrm{AB}}^2 - \Omega^2\big) \\ & - \big(F_y^{\mathrm{dfc}} + D_y\cos\Omega t - D_x\sin\Omega t\big)/m_{\mathrm{A}} \\ & - \big(F_y^{\mathrm{BC}} + F_y^{\mathrm{BD}} - c_{\mathrm{BC}}\dot{y}_{\mathrm{BC}} - c_{\mathrm{BD}}\dot{y}_{\mathrm{BD}} - k_{\mathrm{BC}}y_{\mathrm{BC}} - k_{\mathrm{BD}}y_{\mathrm{BD}}\big)/m_{\mathrm{B}} \end{aligned} \tag{38}$$

$$\begin{aligned} \ddot{x}_{\mathrm{BC}} = {} & 2\dot{y}_{\mathrm{BC}}\Omega + F_x^{\mathrm{BC}}/m_{\mathrm{BC}} - \big(F^{\mathrm{EP}}/2\big)\sin\Omega t/m_{\mathrm{C}} \\ & - (c_{\mathrm{CD}}/m_{\mathrm{C}} + 2\omega_{\mathrm{BC}}\zeta_{\mathrm{BC}})\dot{x}_{\mathrm{BC}} - (c_{\mathrm{BD}}/m_{\mathrm{B}} - c_{\mathrm{CD}}/m_{\mathrm{C}})\dot{x}_{\mathrm{BD}} \\ & - (k_{\mathrm{BD}}/m_{\mathrm{B}} - k_{\mathrm{CD}}/m_{\mathrm{C}})x_{\mathrm{BD}} - \big(k_{\mathrm{CD}}/m_{\mathrm{C}} + \omega_{\mathrm{BC}}^2 - \Omega^2\big)x_{\mathrm{BC}} \\ & - \big(F_x^{\mathrm{AB}} - F_x^{\mathrm{BD}} - c_{\mathrm{AB}}\dot{x}_{\mathrm{AB}} - k_{\mathrm{AB}}x_{\mathrm{AB}}\big)/m_{\mathrm{B}} \end{aligned} \tag{39}$$

$$\ddot{y}_{\mathrm{BC}} = F_y^{\mathrm{BC}}/m_{\mathrm{BC}} - 2\dot{x}_{\mathrm{BC}}\Omega - \left(F^{\mathrm{EP}}/2\right)\cos\Omega t/m_{\mathrm{C}} - (c_{\mathrm{CD}}/m_{\mathrm{C}} + 2\omega_{\mathrm{BC}}\zeta_{\mathrm{BC}})\dot{y}_{\mathrm{BC}} - (c_{\mathrm{BD}}/m_{\mathrm{B}} - c_{\mathrm{CD}}/m_{\mathrm{C}})\dot{y}_{\mathrm{BD}} - (k_{\mathrm{BD}}/m_{\mathrm{B}} - k_{\mathrm{CD}}/m_{\mathrm{C}})y_{\mathrm{BD}} - \left(k_{\mathrm{CD}}/m_{\mathrm{C}} + \omega_{\mathrm{BC}}^2 - \Omega^2\right)y_{\mathrm{BC}} - \left(F_y^{\mathrm{AB}} - F_y^{\mathrm{BD}} - c_{\mathrm{AB}}\dot{y}_{\mathrm{AB}} - k_{\mathrm{AB}}y_{\mathrm{AB}}\right)/m_{\mathrm{B}} \tag{40}$$

$$\ddot{x}_{\mathrm{BD}} = 2\dot{y}_{\mathrm{BD}}\Omega + F_x^{\mathrm{BD}}/m_{\mathrm{BD}} + \left(F^{\mathrm{EP}}/2\right)\sin\Omega t/m_{\mathrm{D}} - (c_{\mathrm{CD}}/m_{\mathrm{D}} + 2\omega_{\mathrm{BD}}\zeta_{\mathrm{BD}})\dot{x}_{\mathrm{BD}} - (c_{\mathrm{BC}}/m_{\mathrm{B}} - c_{\mathrm{CD}}/m_{\mathrm{D}})\dot{x}_{\mathrm{BC}} - (k_{\mathrm{BC}}/m_{\mathrm{B}} - k_{\mathrm{CD}}/m_{\mathrm{D}})x_{\mathrm{BC}} - \left(k_{\mathrm{CD}}/m_{\mathrm{D}} + \omega_{\mathrm{BD}}^2 - \Omega^2\right)x_{\mathrm{BD}} - \left(F_x^{\mathrm{AB}} - F_x^{\mathrm{BC}} - c_{\mathrm{AB}}\dot{x}_{\mathrm{AB}} - k_{\mathrm{AB}}x_{\mathrm{AB}}\right)/m_{\mathrm{B}} \tag{41}$$

$$\ddot{y}_{\mathrm{BD}} = F_y^{\mathrm{BD}}/m_{\mathrm{BD}} + \left(F^{\mathrm{EP}}/2\right)\cos\Omega t/m_{\mathrm{D}} - 2\dot{x}_{\mathrm{BD}}\Omega - (c_{\mathrm{CD}}/m_{\mathrm{D}} + 2\omega_{\mathrm{BD}}\zeta_{\mathrm{BD}})\dot{y}_{\mathrm{BD}} - (c_{\mathrm{BC}}/m_{\mathrm{B}} - c_{\mathrm{CD}}/m_{\mathrm{D}})\dot{y}_{\mathrm{BC}} - (k_{\mathrm{BC}}/m_{\mathrm{B}} - k_{\mathrm{CD}}/m_{\mathrm{D}})y_{\mathrm{BC}} - \left(k_{\mathrm{CD}}/m_{\mathrm{D}} + \omega_{\mathrm{BD}}^2 - \Omega^2\right)y_{\mathrm{BD}} - \left(F_y^{\mathrm{AB}} - F_y^{\mathrm{BC}} - c_{\mathrm{AB}}\dot{y}_{\mathrm{AB}} - k_{\mathrm{AB}}y_{\mathrm{AB}}\right)/m_{\mathrm{B}}. \tag{42}$$

These equations contain the key information about the dynamics of the GG configuration that are not revealed in the two-body analysis of the proposers. In particular, they can be used to explore how drag forces, servo forces, sensor noise and putative EP forces will influence the differential displacements between the test masses. By comparing the effects from disturbances with the effects from an EP violation, the expected performance of the experiment can be assessed, and, moreover, the effects of sensor and actuator noise and misalignments can be incorporated in a realistic manner.

The translational eigenvalues for the uncontrolled four-body system are as follows (omitting the uninteresting spacecraft 'rigid body' modes):

$$\left.\begin{array}{r} -0.279\,9151 - 31.694\,46\mathrm{i} \\ -0.279\,9151 + 31.694\,46\mathrm{i} \\ +0.274\,995 - 31.137\,39\mathrm{i} \\ +0.274\,995 + 31.137\,39\mathrm{i} \end{array}\right\} \text{spacecraft to PGB modes (rad s}^{-1}\text{)}$$

$$\left.\begin{array}{r} -0.035\,422\,92 - 31.451\,87\mathrm{i} \\ -0.035\,422\,92 + 31.451\,87\mathrm{i} \\ +0.035\,341\,96 - 31.379\,99\mathrm{i} \\ +0.035\,341\,96 + 31.379\,99\mathrm{i} \\ -0.029\,921\,56 - 31.477\,32\mathrm{i} \\ -0.029\,921\,56 + 31.477\,32\mathrm{i} \\ +0.029\,805 - 31.354\,53\mathrm{i} \\ +0.029\,805 + 31.354\,53\mathrm{i} \end{array}\right\} \text{PGB to test-mass modes (rad s}^{-1}\text{).}$$

These have been computed for the nominal Q values ($Q_{\mathrm{AB}}^{\mathrm{V}} = 5$, $Q_{\mathrm{BC}}^{\mathrm{V}} = Q_{\mathrm{BD}}^{\mathrm{V}} = 500$). For higher Q values the decay (growth) of stable (unstable) modes would be slower. All the modes are closely spaced in frequency around $\Omega \approx 31.42$ rad s^{-1} (5 Hz), making it virtually impossible to disentangle each unstable mode from the sensor data (in order to re-construct an effective r_w measurement for use in the ideal control law of equation (34)) without incurring unacceptable phase lags and instabilities.

Although all the dynamics of all the modes are coupled, the couplings are sufficiently weak that the control laws can be designed according to the two-body criterion described earlier. The additional control laws required to stabilize the test masses relative to the PGB

are

$$\begin{pmatrix} F_x^{\mathrm{BC}} \\ F_y^{\mathrm{BC}} \end{pmatrix} = -C_{\mathrm{BC}} \begin{pmatrix} 1+\delta_{\mathrm{BC}}^{F_x} & 0 \\ 0 & 1+\delta_{\mathrm{BC}}^{F_y} \end{pmatrix} \begin{pmatrix} \cos\epsilon_{\mathrm{BC}}^{F} & \sin\epsilon_{\mathrm{BC}}^{F} \\ -\sin\epsilon_{\mathrm{BC}}^{F} & \cos\epsilon_{\mathrm{BC}}^{F} \end{pmatrix} \begin{pmatrix} \hat{\hat{x}}_{\mathrm{BC}} - \Omega\hat{y}_{\mathrm{BC}} \\ \hat{\hat{y}}_{\mathrm{BC}} + \Omega\hat{x}_{\mathrm{BC}} \end{pmatrix} \tag{43}$$

and similarly for the (B, D) pair, where the scale-factor errors and misalignments are defined as for the (A, B) pair described earlier. The control gains for the additional electrostatic servos are given by

$$C_{\mathrm{BC}} = g_{\mathrm{BC}} \frac{\sqrt{k_{\mathrm{BC}} m_{\mathrm{BC}}}}{Q_{\mathrm{BC}}^{\mathrm{V}}} \frac{\Omega}{\omega_{\mathrm{BC}}}, \qquad C_{\mathrm{BD}} = g_{\mathrm{BD}} \frac{\sqrt{k_{\mathrm{BD}} m_{\mathrm{BD}}}}{Q_{\mathrm{BD}}^{\mathrm{V}}} \frac{\Omega}{\omega_{\mathrm{BD}}} \tag{44}$$

with $g_{\mathrm{AB}} = g_{\mathrm{BC}} = g_{\mathrm{BD}} \approx 1.2$ found to be reasonable. Note that the gains depend directly on the effective viscous losses in the rotating frame ($Q_{\mathrm{AB}}^{\mathrm{V}}$, $Q_{\mathrm{BC}}^{\mathrm{V}}$, $Q_{\mathrm{BD}}^{\mathrm{V}}$).

The complete set of 12 sensor measurement equations including all noise terms, scale-factor errors, angular misalignments, and lead–lag filters are constructed in direct analogy with those in section 2.2.6 and are not reproduced here.

2.3.2. Drag-free control. The spacecraft inertial acceleration will couple into the differential science signal due to misalignments and imbalances in the mechanical suspensions and electrostatic servo systems. The largest contribution is the aerodynamic drag. This can be attenuated by the technique of drag-free control, whereby a measurement of the relative displacement between the spacecraft and the PGB can be used in a feedback law to command thrusters mounted on the spacecraft. A reasonable choice of control law would be, in the inertial frame,

$$\vec{F}_{\mathrm{ideal}}^{\mathrm{dfc}} = \left(K_{\mathrm{P}}^{\mathrm{dfc}\,n} x_{\mathrm{AB}} + K_{\mathrm{D}}^{\mathrm{dfc}\,n} \dot{x}_{\mathrm{AB}}\right)\vec{n}_1 + \left(K_{\mathrm{P}}^{\mathrm{dfc}\,n} y_{\mathrm{AB}} + K_{\mathrm{D}}^{\mathrm{dfc}\,n} \dot{y}_{\mathrm{AB}}\right)\vec{n}_2. \tag{45}$$

Again, the control must be implemented in the rotating frame (since the sensors and the thrusters are fixed in the spacecraft). Under transformation, the control law becomes

$$\vec{F}_{\mathrm{design}}^{\mathrm{dfc}} = \left(K_{\mathrm{P}}^{\mathrm{dfc}} x_{\mathrm{AB}} + K_{\mathrm{D}}^{\mathrm{dfc}}(\dot{x}_{\mathrm{AB}} - \Omega y_{\mathrm{AB}})\right)\vec{a}_1 + \left(K_{\mathrm{P}}^{\mathrm{dfc}} y_{\mathrm{AB}} + K_{\mathrm{D}}^{\mathrm{dfc}}(\dot{y}_{\mathrm{AB}} + \Omega x_{\mathrm{AB}})\right)\vec{a}_2. \tag{46}$$

This will also be subject to sensor and actuator errors, analogous to those described in section 2.2.6 for the internal servo forces. An important consequence is that both components of drag (D_x and D_y) are coupled into both components of the differential science signal, the net result being that the main drag term D_x dominates the error budget, despite the fact that it acts orthogonal to the EP signal in inertial space.

The minimal required drag-free control gains $\left(K_{\mathrm{P}}^{\mathrm{dfc}}, K_{\mathrm{D}}^{\mathrm{dfc}}\right)$ can be determined from the stability criterion:

$$\left(\frac{c_{\mathrm{AB}}}{m_{\mathrm{AB}}} + \frac{K_{\mathrm{D}}^{\mathrm{dfc}}}{m_{\mathrm{A}}}\right)^2 \left(\frac{k_{\mathrm{AB}}}{m_{\mathrm{AB}}} + \frac{K_{\mathrm{P}}^{\mathrm{dfc}}}{m_{\mathrm{A}}}\right) > \Omega^2 \left(\frac{c_{\mathrm{AB}}}{m_{\mathrm{AB}}}\right)^2 \tag{47}$$

where it is assumed that the non-rotating damping is de-activated ($C_{\mathrm{AB}} = 0$) when the drag-free control is operational (this is found to be preferable in terms of disturbance rejection). In addition to meeting the stability requirement, the gains should be chosen high enough to reject the steady-state drag ($D\rfloor_{\mathrm{dc}} = \sqrt{D_x\rfloor_{\mathrm{dc}}^2 + D_y\rfloor_{\mathrm{dc}}^2}$) which occurs effectively at DC in inertial space. A practical upper limit is dictated by the minimum response time of the thruster drive electronics, and by the need to avoid excessive sensor noise amplification and/or excitation of spacecraft structural modes. Reasonable gain values are found to be $K_{\mathrm{P}}^{\mathrm{dfc}} \approx 6.5 \times 10^5$ N m^{-1}, $K_{\mathrm{D}}^{\mathrm{dfc}} \approx 1.26 \times 10^4$ N s m^{-1}, giving a drag-free closed-loop bandwidth of approximately 12 Hz. Although the drag-free control is required for attenuating the principal external forces, it does introduce additional disturbances near the

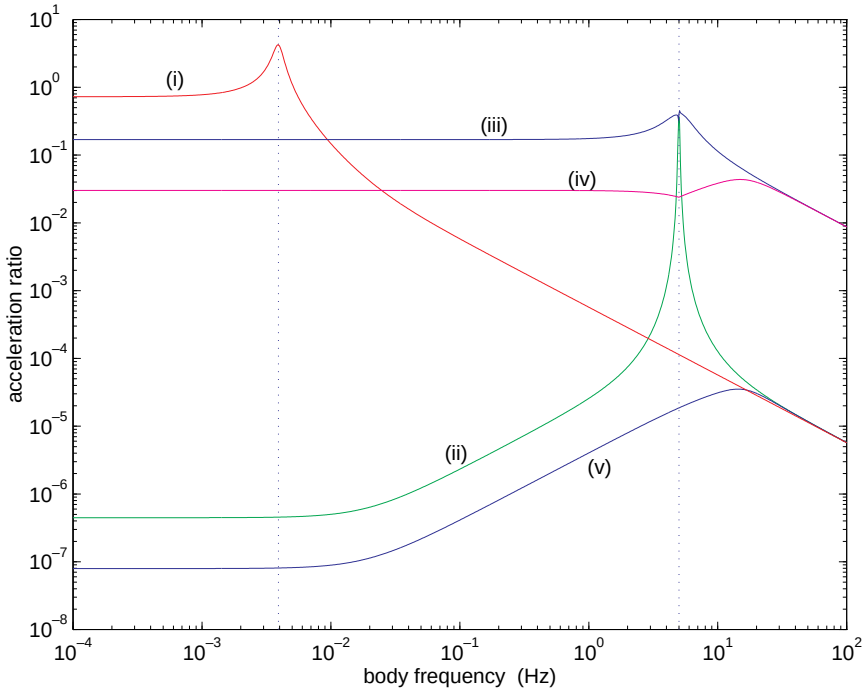

Figure 3. Inertial acceleration of the PGB in response to spacecraft-induced disturbances, e.g. due to thruster system errors, vibration, etc. The various curves, corresponding to different parameter values, were computed as follows: given the two components of body-fixed spacecraft disturbance acceleration occurring at body frequency ω (2π times abscissa), the two components of the inertial accelerations of the PGB are calculated. These are produced at $[\Omega + \omega]$ and at $[\Omega - \omega]$, not at ω. The plotted 'transfer functions' are obtained by using the matrix norm induced by vector norms l_1 and l_∞ (which are the same here) of the 2×2 transfer matrix. Hence they show the maximum transmission factors from input vector at ω to output at either or both $[\Omega + \omega], [\Omega - \omega]$. Curve (i) is for zero spin rate with no servo forces and no drag-free control. This is simply the classical result for an elastic suspension. Curve (ii) is for 5 Hz spin, but with no servo forces and no drag-free control. *This system is unstable*. Curve (iii) is for 5 Hz spin, with the required non-rotating damping servo forces, but no drag-free control. Curve (iv) is for 5 Hz spin, with non-rotating damping servo forces and drag-free control. Curve (v) is for 5 Hz spin, with drag-free control with 12 Hz bandwidth, but no non-rotating damping servo forces. The plot resolution is too coarse to reveal the twin-peak structure in curves (ii)–(v) arising from the weak passive suspension. The vertical lines indicate the natural frequency of the suspension (0.004 Hz), and the spin frequency (5 Hz), respectively. It is clear from these plots, especially curve (iii), that the rapidly rotating PGB offers no significant attenuation of spacecraft vibrations. The drag-free control laws themselves provide the necessary attenuation. (This figure can be viewed in colour in the electronic version of the article; see `http://www.iop.org`)

signal frequency due to imperfections in the thruster system. However, as shown in curve (v) of figure 3, the drag-free control laws themselves are highly effective in attenuating these self-induced disturbances. The figure shows the appropriate 'transfer functions' relating the resultant PGB inertial acceleration due to applied disturbances generated by the spacecraft in the rotating frame, for various cases (see the figure caption for a detailed explanation of the curves). It has been suggested by the proposers that the PGB is useful for attenuating these high-frequency disturbances, basing their argument on the attenuation properties of

weak passive suspension at zero spin (curve (i), figure 3). However, the claim is not valid in the rapidly spinning spacecraft (as demonstrated by curves (ii)–(v), figure 3). The PGB alone offers no significant attenuation of vibrations, particularly around the spin frequency, and could in fact be omitted.

2.3.3. State-space form of dynamical equations and control laws. The entire system of dynamical equations plus all control laws and sensor equations can be expressed compactly in state-space form

$$\dot{\boldsymbol{X}} = \boldsymbol{A}\boldsymbol{X} - \boldsymbol{B}_{\mathrm{C}}\boldsymbol{K}\boldsymbol{X} + \boldsymbol{B}_{\mathrm{D}}\boldsymbol{U}_{\mathrm{D}} + \boldsymbol{B}_{\mathrm{N}}\boldsymbol{N} \tag{48}$$

where the state vector $\boldsymbol{X}$ contains all the actual states, the estimated states, plus the additional states associated with the lead–lag filters; the external force vector $\boldsymbol{U}_{\mathrm{D}}$ contains the drag and EP forces; the noise vector $\boldsymbol{N}$ contains all the sensor noise and thruster noise components; and the gain matrix $\boldsymbol{K}$ contains all the control gains. With this formulation, it is straightforward to determine the closed-loop transfer functions which describe how the drag, sensor noise, thruster noise and putative EP forces will contribute to the two components of measured differential displacement in the PGB reference frame. Since the drag and EP forces act in the inertial frame, it is necessary to evaluate the transfer functions for both quadrature components separately, then take account of the phase differences when combining them.

2.3.4. 'Common-mode rejection'. When assessing the effects of drag, the transfer functions of interest are those which describe the test-mass differential displacements in the PGB frame corresponding to the DC inertial drag forces

$$\left|G_x^{D_x}\right| \triangleq \left|\frac{\Delta x(\omega = \Omega)}{D_x\rfloor_{\mathrm{dc}}/m_{\mathrm{A}}}\right|, \qquad \left|G_y^{D_x}\right| \triangleq \left|\frac{\Delta y(\omega = \Omega)}{D_x\rfloor_{\mathrm{dc}}/m_{\mathrm{A}}}\right| \tag{49}$$

and similarly for $\left|G_x^{D_y}\right|, \left|G_y^{D_y}\right|$. Evaluating these expressions for the full system in equation (48) gives a measure of the total common-mode rejection including the combined effects of mechanical suspension imbalances and mismatches in the servo control forces. The corresponding transfer functions for the body-fixed differential displacements resulting from an EP violating force are

$$\left|G_x^{\mathrm{EP}}\right| \triangleq \left|\frac{\Delta x(\omega = \Omega)}{F^{\mathrm{EP}}/m_{\mathrm{D}}}\right| \qquad \left|G_y^{\mathrm{EP}}\right| \triangleq \left|\frac{\Delta y(\omega = \Omega)}{F^{\mathrm{EP}}/m_{\mathrm{D}}}\right|. \tag{50}$$

The expected EP measurement performance (Eötvös ratio) for a given level of drag is therefore given by

$$\eta_x^{\mathrm{D}} = \frac{\mathrm{SNR}}{g}\frac{\left|G_x^{D_x}\right|(D_x\rfloor_{\mathrm{dc}}/m_{\mathrm{A}}) + \left|G_x^{D_y}\right|(D_y\rfloor_{\mathrm{dc}}/m_{\mathrm{A}})}{\left|G_x^{\mathrm{EP}}\right|} \tag{51}$$

and similarly for the orthogonal component η_y^{D}, where SNR is the desired signal-to-noise-ratio and g is the Earth's gravitational acceleration.

2.3.5. Sensor noise propagation. Similarly, the effects of sensor noise propagation into the differential signals can be assessed. In this case, there are 12 transfer functions to be evaluated (corresponding to six sensors propagating into Δx and Δy). After computing the transfer functions, the combined effect of all six noise components on each of $\Delta x, \Delta y$ can be approximated by assuming that all the sensor noises are uncorrelated 'white noise'. Then,

the net effect can be determined by simply adding the power spectra of the individual terms. If it is further assumed that the noise terms have approximately equal spectral densities, an effective transfer function can be obtained from the individual transfer functions for each direction

$$\left|G_x^{\mathrm{N}}\right| = \sqrt{\sum_{j=6}^{n}\left|G_x^{n_j}\right|^2}, \qquad \left|G_y^{\mathrm{N}}\right| = \sqrt{\sum_{j=6}^{n}\left|G_y^{n_j}\right|^2}. \tag{52}$$

Then, the effective EP measurement sensitivities in the presence of sensor noise can be computed from

$$\eta_x^{\mathrm{N}} = \frac{\mathrm{SNR}}{g}\frac{\left|G_x^{\mathrm{N}}\right|\sqrt{\Phi_n}}{\left|G_x^{\mathrm{EP}}\right|}\frac{1}{\sqrt{\Delta T}} \tag{53}$$

and similarly for η_y^{N}, where $\sqrt{\Phi_n}$ is the square root of the power spectral density of each component of sensor noise and ΔT is the averaging time.

2.3.6. Expected EP measurement performance. The effects of drag and sensor noise can be combined to give an effective measurement sensitivity in each coordinate direction, and the expected experiment performance is taken as the better of these two, i.e.

$$\eta_{\mathrm{exp}} \approx \min\left\{\left[\eta_x^{\mathrm{D}} + \eta_x^{\mathrm{N}}\right], \left[\eta_y^{\mathrm{D}} + \eta_y^{\mathrm{N}}\right]\right\}. \tag{54}$$

For the main drag forces and for the sensor noise spectral density, numerical values have been taken from the GG proposal [2], i.e. $D_x\rfloor_{\mathrm{dc}} = 1.535 \times 10^{-5}$ N, $D_y\rfloor_{\mathrm{dc}} = 9.6 \times 10^{-8}$ N, $\sqrt{\Phi_n} = 3 \times 10^{-12}$ m Hz$^{-1/2}$. Note that these drag values are very optimistic, assuming the best-case solar minimum conditions. The drag may well be orders of magnitude higher at the proposed altitude of 520 km.

The sensor, actuator and thruster misalignments ($\epsilon_{\mathrm{AB}}^{F}$, $\epsilon_{\mathrm{AB}}^{S}$, etc), are assumed to be of the order of 10^{-4} rad, and the scale-factor errors, ($\delta_{\mathrm{AB}}^{S_x}$, $\delta_{\mathrm{AB}}^{S_y}$, etc) of the order of 10^{-3} rad. These values should be considered as optimistic, since they incorporate the combined effects of all electronic and mechanical imperfections.

An SNR value of 2 has been used, to be consistent with the proposal [2]. However, this is rather marginal, and a value of 6 or higher is required to make a convincing measurement. For the averaging time ΔT, the value of 12 h has been used, again, to be consistent with the proposal [2].

The expected EP measurement performance was evaluated via equations (49)–(54) computed for the full system in equation (48) using the numerical parameters stated above. The results obtained are summarized as follows: (i) without drag-free control, the best-case performance is $\eta_{\mathrm{exp}} = 10^{-11}$, irrespective of the assumptions for Q^{V}. Drag-free control is therefore essential. This is in sharp contrast with the views expressed in earlier versions of the GG proposal [5], where drag-free control was explicitly excluded. They proposed that the passive suspension could be balanced by an ultra-precise on-orbit trimming system thereby achieving a mechanical common-mode rejection many orders of magnitude better than the already optimistic values used in the present analysis; (ii) with drag-free control, where the gains are chosen to balance the effects of drag and sensor noise propagation, but without exceeding the practical upper limit on the closed-loop bandwidth of around 12 Hz, the resulting performances are as follows, depending on the assumed values for Q^{V} (see table 1): (i) for nominal Q^{V} ($Q_{\mathrm{AB}}^{\mathrm{V}} = 5$, $Q_{\mathrm{BC}}^{\mathrm{V}} = Q_{\mathrm{BD}}^{\mathrm{V}} = 500$), the best-case performance is $\eta_{\mathrm{exp}} = 2 \times 10^{-13}$; (ii) for high Q^{V} ($Q_{\mathrm{AB}}^{\mathrm{V}} = 5$, $Q_{\mathrm{BC}}^{\mathrm{V}} = Q_{\mathrm{BD}}^{\mathrm{V}} = 2.5 \times 10^4$), the best-case performance is $\eta_{\mathrm{exp}} = 10^{-14}$; (iii) for extreme Q^{V} ($Q_{\mathrm{AB}}^{\mathrm{V}} = 5$, $Q_{\mathrm{BC}}^{\mathrm{V}} = Q_{\mathrm{BD}}^{\mathrm{V}} = 2.5 \times 10^5$), the

best-case performance is $\eta_{\rm exp} = 10^{-15}$. In all cases when the drag-free control is enabled the non-rotating damping between the spacecraft and PGB should be de-activated, since it degrades the drag rejection and the experimental performance.

The values used above for $Q^{\rm V}$ were taken from the GG proposal [2]. After the draft of this paper was submitted, new experimental structural loss factors were announced by the proposers: $\frac{1}{90}$ for the PGB springs, and $\frac{1}{16\,000}$ for the test-mass springs. If it is assumed for the sake of argument that the spring losses would be the only source of dissipation in the entire system, and that the idealized model of pure structural damping is applicable (see the appendix), then the equivalent viscous Q values are $Q^{\rm V}_{\rm AB} = 10^5$ and $Q^{\rm V}_{\rm BC} = Q^{\rm V}_{\rm BD} = 10^7$. Even under these extremely optimistic assumptions, the ultimate performance of the experiment, according to the present analysis, will still be no better than $\eta = 10^{-15}$. In other words, the experimental performance does not improve for $Q^{\rm V}$ values in excess of $\approx 10^5$. This is because, in the presence of unavoidable misalignments, the residual drag and sensor noise propagating through the drag-free control system enter the differential mode, regardless of the level of $Q^{\rm V}$ between the inner bodies. This important result can only be obtained from the four-body analysis presented here, and is not discussed in [1–3], where only a two-body analysis is considered.

2.3.7. Three-dimensional effects and other considerations. The simplified planar models presented above neglect all 3D dynamical effects. However, it is clear that such effects will be important, and will generally degrade the experimental performance further. For example, as noted earlier, the rotational dynamics of each body must be precisely controlled. For simplicity, perfect control was assumed here, but the consequences of imperfect control must be considered in a more complete error budget. Furthermore, it is likely that the other degrees of freedom in attitude of each body will be excited by actuator imbalances and transients, and will also require control, with a consequent increase in system complexity. As another example, the thin connecting rods proposed in [1–3] are dynamically unstable (since they are rotating about their axes of minimum inertia). It is straightforward to show that the torques required to stabilize the rods, when expressed in terms of stiffness of the springs connecting the rods to the test masses, would be many orders of magnitude higher than the stiffnesses proposed. This will have a significant impact on the system dynamics. Subsequent to the present analysis, the GG proposers revised their design to incorporate stabilizing discs to enhance the inertias of the rods about their spin axes, thus providing passive stability. Even if the revised geometries could be accommodated, the resulting rods will have non-negligible mass and inertias. Since they are connected directly to the test masses, the dynamics of the test masses and the common mode rejection will be affected. A complete 3D analysis is required to assess the consequences on the experimental performance. Likewise, all other contributions to the error budget, not related to the dynamics and control aspects covered here, must be included (for example, the effects of thermal noise, residual gas pressure, temperature gradients and other sources of parasitic force). It is important to note that the practical implementation of the required drag-free control on a rapidly rotating spacecraft is considerably more demanding than on a slowly rotating (or non-rotating) spacecraft. Likewise, the requirement for attitude, rotation and 'non-rotating damping' laws for all internal bodies leads to an extremely complicated system. Furthermore, as currently proposed, GG has only one pair of test masses, so it is impossible to discriminate against systematic errors in the science signal. This is a serious shortcoming.

3. Conclusions

It is found that the GG experiment as proposed in [1–3] is limited by the imperfections inherent in the practical implementation of the control forces required for rejecting drag and for stabilizing the system at supercritical speeds. The key limiting factors are (i) the inaccuracy in the balancing of the servo forces which determines the degree of coupling of the residual drag into the differential mode, and (ii) the propagation of sensor noise into the differential mode. It is shown that high-gain drag-free control is essential for the experiment to be of scientific interest, and, furthermore, that the proposed passive isolation stage (the PGB) offers no useful attenuation of spacecraft-generated disturbances near the signal frequency in the rapidly rotating spacecraft, and could be omitted. Calculations based on an analytical model of the free-flying four-body system suggest that the expected EP measurement performance is $\eta \approx 10^{-14}$ under realistic assumptions for the effective imperfections and losses in the system. Even with extremely optimistic damping models which lead to very high effective Q values, the experiment performance would not significantly improve because residual drag and noise in the drag-free control system become the dominant error contributions, and these are basically unaffected by the high Q values. The system is found to be technically complex, requiring the implementation of many interacting control systems in a rapidly rotating spacecraft. The need to incorporate more test masses to eliminate systematic errors must be addressed, with the consequent implications on additional system complexity. This study focused on the 2D dynamical effects. A more complete analysis would require a full consideration of the 3D dynamical effects and all other pertinent error sources.

Appendix. Structural and viscous losses in supercritical rotation

To assess the level of the required active stabilizing forces it is necessary to know the total destabilizing rotating damping force at the operating frequency of 5 Hz. Experimentation on a test system which is geometrically and operationally similar to the flight system (i.e. rotating at 5 Hz with powered-up sensors and actuators) is the most reliable approach. This would avoid the need to apply approximate scaling laws to different simplified models of the various loss mechanisms. Such experiments would be very difficult owing to the necessity for isolating the rotating test system from the (beneficial) losses due to interaction with the inertial (laboratory) frame. Furthermore, it is highly challenging to perform such measurements on a system with very weak springs which must be suspended in the terrestrial 1 g environment. In the absence of such direct experimental results, damping phenomena can be measured or estimated individually at different operating conditions, then scaled using approximate laws, in order to estimate the total damping at full operational conditions where there may be coupling between the various loss effects. The scaling laws are based on models which are known to be imperfect [7, 8]. To evaluate the consequences of coexisting types of damping that are approximated by structural and viscous models, the following considerations are pertinent.

Here we adopt the notation used in [7] to aid comparison between our results and the approach taken by the GG proposers. Consider the general case where c_r represents the viscous damping coefficient in the rotating frame, and c_n represents the viscous damping coefficient in the inertial frame ('non-rotating damping'). It is understood that c_n includes all non-rotating damping, passive or active. Then, the simplified characteristic equation for an elastically suspended rotor spinning at a constant rate Ω, written in the inertial frame,

using complex notation is

$$mS^2 + (c_n + c_r)S + k - \mathrm{i}\Omega c_r = 0. \tag{A1}$$

This is the same as equation (4-19) in [7]. Now consider that there is 'structural damping' in the material. Then, the stiffness can be approximated by

$$k = k_0(1 - \mathrm{i}\eta) \tag{A2}$$

where η is the 'modulus defect'†, and can be defined as $\eta \approx 1/Q^*$ where Q^* is the 'intrinsic Q' of the material, assuming that anelasticity is the dominant effect. The appropriate condition for stability (for the forward modes) is

$$\frac{c_n}{m} + \frac{c_r}{m} > \frac{|-\eta k_0/m - \Omega c_r/m|}{\sqrt{k_0/m}} = \frac{\left|\eta\omega_n^2 + \Omega c_r/m\right|}{\omega_n} \qquad \text{where} \quad \omega_n \triangleq \sqrt{k_0/m}. \tag{A3}$$

This is a more general result than expressed in section 4.5.5 of [7] because it allows for both structural and viscous contributions to the rotating damping.

Consider now the idealized case where there is no viscous rotating damping ($c_r = 0$), then the stability criterion becomes

$$c_n > \omega_n m\eta = \frac{\sqrt{k_0 m}}{Q^*} \tag{A4}$$

which is the result quoted in [7] and used in the GG proposal [2]. Then, the ratio of active forces to passive forces is given by

$$F^{\text{ratio}} \triangleq \frac{c_n \Omega \Delta x}{k_0 \Delta x} = \frac{1}{Q^*}\left(\frac{\Omega}{\omega_n}\right) \approx \frac{628}{Q^*}. \tag{A5}$$

For nominal parameter values, this becomes $F^{\text{ratio}} \approx 1.3$ for $Q^* = 500$, $F^{\text{ratio}} \approx 2.5 \times 10^{-2}$ for $Q^* = 2.5 \times 10^4$ (a measured low-frequency value for Be–Cu at room temperature [10, 11]), and $F^{\text{ratio}} \approx 2.5 \times 10^{-3}$ for $Q^* = 2.5 \times 10^5$ (a measured high-frequency value for Be–Cu at room temperature [12]). Indeed, for the high values of Q^*, these results suggest that the active servo forces (neglecting noise) are relatively small compared with the passive spring forces. Note, however, that this result is not as favourable as implied by the impractical idealized control law of equation (34).

If, on the other hand, it is assumed that there is no structural damping ($\eta = 0$), and only rotating viscous damping, then, equation (A3) gives equation (27) as the condition for stability. The force ratio then becomes equation (30) (with $g_{\text{AB}} = 1$) which is worse than in equation (A5) by a further factor of (Ω/ω_n) (for Q^{V} of the same order as Q^*).

In order to determine which F^{ratio} is valid, i.e. equation (A5), or the less favourable equation (30), one has to assess which rotating damping effect is dominant: pure structural or pure viscous? This can be answered by re-inspection of equation (A3), and checking the condition for when the relative contributions of structural damping and viscous damping are equal. This reveals

$$c_r^{\text{equiv}} = \frac{\eta k_0}{\Omega} = \frac{k_0}{Q^*\Omega}. \tag{A6}$$

Expressing in terms of Q^{V}, the condition for which viscous rotating damping dominates is given by

$$Q^{\text{V}} < \frac{\sqrt{k_0 m}}{c_r^{\text{equiv}}} = \Omega Q^* \sqrt{\frac{m}{k_0}} = Q^*\left(\frac{\Omega}{\omega_n}\right) \tag{A7}$$

† Not to be confused with main text where η represented the Eötvös ratio.

which demonstrates that as long as Q^{V} is less than 6.3×10^6 for $Q^* \approx 10^4$, or Q^{V} is less than 6.3×10^7 for $Q^* \approx 10^5$, then the viscous rotating damping will dominate, and the less favourable force ratio in equation (30) is the valid one. The actual value of Q^{V} depends on various contributions including viscous-like losses in the material itself, in any joints between springs and bodies and in the electronic circuits for the sensors and actuators. The various processes are complicated to model, and all are known to have a frequency dependence. Experimentation is the most reliable approach to determine the total Q^{V} from all sources. In any case, it is extremely unlikely that an electromechanical system can yield viscous Q values higher than 10^6 or so at 5 Hz. It is therefore concluded that the viscous damping (in the rotating frame) will dominate, and so the less favourable ratio of forces prevails (equation (30)). In our investigation, we therefore report results for three different sets of values of Q^{V}: (i) the nominal-Q case, where $Q^{\mathrm{V}}_{\mathrm{BC}} = Q^{\mathrm{V}}_{\mathrm{BD}} = 500$ are taken at their low-frequency face values, as originally suggested by the GG proposers; (ii) the high-Q case, where $Q^{\mathrm{V}}_{\mathrm{BC}} = Q^{\mathrm{V}}_{\mathrm{BD}} = 2.5 \times 10^4$, based on highly optimistic frequency-scaling assumptions; (iii) the extreme-Q case, where $Q^{\mathrm{V}}_{\mathrm{BC}} = Q^{\mathrm{V}}_{\mathrm{BD}} = 2.5 \times 10^5$ and even 10^7 (see section 2.3.6), consistent with the values recently proposed. It is assumed that the effective $Q^{\mathrm{V}}_{\mathrm{AB}}$ for for the spacecraft-to-PGB coupling will not be very high since these springs must communicate all the electrical power and signals to the experiment, and are thus likely to be lossy.

References

[1] Nobili A *et al* 1995 *J. Astronaut. Sci.* **43** 219–42
[2] Nobili A *et al* 1996 *GG Pre-Phase A Report* unpublished report, University of Pisa
[3] Nobili A, Bramanti D and Catastini G 1996 *Class. Quantum Grav.* **13** A197–201
[4] Lange B O 1964 *Am. Inst. Aeronaut. Astronaut. J.* **2** 1590–606
[5] Bramanti D, Nobili A and Catastini G 1992 *Phys. Lett.* **164A** 243–54
See also Nobili A *et al* 1993 Proposal for the M3 medium size mission of ESA
[6] Su Y, Heckel B R, Adelberger E G, Gundlach J H, Harris M, Smith G L and Swanson H E 1994 *Phys. Rev.* D **50** 3614–36
[7] Genta G 1993 *Vibration of Structures and Machines* (Berlin: Springer)
[8] Crandall S H 1970 *J. Sound Vib.* **11** 3–18
[9] Crandall S H 1997 Private communication
[10] Quinn T J and Speake C C 1992 *Phil. Mag.* A **65** 261
[11] Quinn T J, Speake C C, Davis R S and Tew W 1995 *Phys. Lett.* **197A** 197–208
[12] Duffy W 1992 *Cryogenics* **32** 1121